Modeling of brittle failure based on a Hoek & Brown yield criterion parametric studies and constitutive validation

Marinelli, F; Zalamea, N.; Vilhar, Gregor; Brasile, S.; Cammarata, G.; Brinkgreve, Ronald

Publication date
2019

Document Version
Final published version

Published in
Proceedings of the 53rd US Rock Mechanics / Geomechanics Symposium

Citation (APA)
Marinelli, F., Zalamea, N., Vilhar, G., Brasile, S., Cammarata, G., & Brinkgreve, R. (2019). Modeling of brittle failure based on a Hoek & Brown yield criterion: parametric studies and constitutive validation. In *Proceedings of the 53rd US Rock Mechanics / Geomechanics Symposium: New York, 23-26 June 2019* Article ARMA 19–410 American Rock Mechanics Association (ARMA).

ARMA 19–410

Modeling of brittle failure based on a Hoek & Brown yield criterion: parametric studies and constitutive validation

Marinelli, F.
Plaxis bv, a Bentley Systems company, Delft, Netherlands
Zalamea, N.
Université Grenoble Alpes, 3SR, F-38000, Grenoble, France
Vilhar, G., Brasile, S., Cammarata, G. and Brinkgreve, R.
Plaxis bv, a Bentley Systems company, Delft, Netherlands

This paper was prepared for presentation at the 53rd US Rock Mechanics/Geomechanics Symposium held in New York, NY, USA, 23–26 June 2019. This paper was selected for presentation at the symposium by an ARMA Technical Program Committee based on a technical and critical review of the paper by a minimum of two technical reviewers. The material, as presented, does not necessarily reflect any position of ARMA, its officers, or members. Electronic reproduction, distribution, or storage of any part of this paper for commercial purposes without the written consent of ARMA is prohibited. Permission to reproduce in print is restricted to an abstract of not more than 200 words; illustrations may not be copied. The abstract must contain conspicuous acknowledgement of where and by whom the paper was presented.

ABSTRACT: Hoek & Brown (HB) failure criteria have been employed over the past decades in common engineering applications due to their extended capability to capture the non-linear yielding of different types of rocks. Often implemented within a perfect plastic framework, this constitutive approach is here enhanced by introducing a softening rule to simulate the post-peak behaviour of rocks in the brittle regime. For this purpose, the degradation of the material properties has been expressed as a function of an internal variable (i.e., the cumulated value of deviatoric plastic strains) which allows one to simulate the rock failure resulting from dilating shearing. Furthermore, to accurately describe the non-linear dilatancy after the peak, the same hyperbolic trend has been applied also to the material properties governing the expression of the plastic potential. The performance of these constitutive equations has been inspected through parametric analyses to emphasize the role of the softening parameters at material point level, as well as to study the strain localization potential of the Hoek & Brown model with Softening (HBS). As a further validation, the shear band angles predicted with the theory have been compared by performing the same tests with finite element code PLAXIS 2D, thus confirming the model capability to simulate failure mechanisms within a strain localization regime.

1. INTRODUCTION

To describe the influence of joints, fractures and discontinuities on the mechanical behaviour of rock masses, the approach proposed by Hoek & Brown (HB) has been successfully employed over the past decades in common engineering applications, thus enabling their mechanical characterization within a continuum framework (Hoek, 1983; Hoek, 1990; Hoek and Brown, 1997; Martin et al., 1999; Hoek et al., 2002 and Eberhardt, 2012). The main advantage of this constitutive approach is to provide a useful link between the theoretical framework of the elasto-plastic theory and the geological practice commonly used for the qualitative assessment of rock mass properties (e.g., the GSI system detailed by Marinos et al., 2005; Cai et al., 2004; Cai et al., 2007, and Cai, 2010).

Although efficiently employed to solve practical problems (Carranza-Torres and Fairhurst, 1999; Zhao and Cai, 2010 and Cai, 2011), the HB approach has been mainly used within a perfect plastic framework, thus preventing further mechanisms of failure resulting from material softening, which can potentially compromise the behaviour of geo-engineering structures. To overcome this limitation, several formulations have been recently proposed (Alejano et al., 2010; Zou et al., 2016 and Lin et al., 2018) which consider the HB yielding with a piece-wise linear decrease of the material strength. Along these lines, the goal of this study is to define a different decay of the post-peak response by introducing a hyperbolic decrease of the material properties (Barnichon, 1998; Collin, 2002) to guarantee a smoother transition between the peak stress and the corresponding residual behaviour. Furthermore, the same hyperbolic expression has been used to model a non-linear variability of dilation (i.e., the formulation proposed by El Moustapha, 2014), thus obtaining a more accurate trend of volumetric strain in the brittle regime. After calibrating the model parameters to simulate the mechanical behaviour of a porous rock (i.e., Rothbach sandstone), the performance of the selected constitutive equations has been inspected through parametric analyses with emphasis on the parameters which govern the rate of softening and the rate of dilation, respectively. Furthermore, to investigate the capability of the implemented model, the strain localization theory (Rudnicki and Rice, 1975) has been employed to study possible failure mechanisms through the formation of potential shear bands. The theoretical results have been validated with numerical solutions obtained by solving

the same stress paths as an Initial Boundary Value Problem (IBVP) by using PLAXIS 2D, thus confirming the predicted values of the band angle with the numerical solution computed with FE analyses.

2. CONSTITUTIVE FORMULATION: A HOEK & BROWN MODEL WITH SOFTENING (HBS)

The elasto-plastic characteristics of the Hoek & Brown with softening (HBS) have been defined according to the yield surface proposed by Jiang and Zhao, 2015 which represents a generalization of the Hoek & Brown criterion through the invariants associated with the stress tensor:

$$f = \frac{q^{1/a}}{\sigma_{ci}^{(1/a-1)}} + A(\theta)\frac{q}{3}m_b - m_b p - s\sigma_{ci}, \qquad (1)$$

Where p, q and θ represent the mean stress (i.e., $p = (\sigma_{xx} + \sigma_{yy} + \sigma_{zz})/3$), the stress deviator (i.e., $q = \sqrt{1.5(s_{ij}s_{ij})}$ where $s_{ij} = \sigma_{ij} - p\delta_{ij}$ is the deviator component of σ_{ij} and δ_{ij} represents the Kronecker's symbol) and the Lode angle (i.e., $cos(3\theta) = \sqrt{6}tr(s^3)/tr(s^2)^{3/2}$), respectively. In Eq. 1, the function $A(\theta)$ is defined according to the formulation proposed by Jiang and Zhao, 2015 in which $A(\theta) = 2\cos(\pi\backslash 3 - \theta)$ and σ_{ci} represents the uniaxial compression strength. m_b, s and a are dimensionless parameters which are determined through the empirical correlations proposed by Marinos el al., 2015 and Brown, 2008 (i.e., the GSI system):

$$m_{b_i} = m \cdot \exp\left(\frac{GSI - 100}{28 - 14D}\right),$$
$$s_i = \exp\left(\frac{GSI - 100}{9 - 3D}\right), \qquad (2)$$
$$a = \frac{1}{2} + \frac{1}{6}\left(e^{-GSI/15} - e^{-20/3}\right),$$

where GSI represents the Geological Strength Index which is aimed to determine the quality of the rock mass from geological observations of joints, fractures and discontinuities. Although the GSI classification enables to differentiate the initial yielding according to the spatial distribution of discontinuities, there is no specific reference to their rock-quality (i.e., the opening and the roughness of joints and fractures). For this purpose, a disturbance factor D has been introduced by Hoek et al., 2002 to calculate the material properties m_b, s and a, as reported in Eq. 2.

According to the elasto-plastic theory, plastic strains ε_{ij}^p are computed by using the classical flow rule: $\varepsilon_{ij}^p = \lambda(\partial g/\partial\sigma_{ij})$, where λ represents the plastic multiplier and g the plastic potential, respectively. To introduce non-associative plasticity in the constitutive equations, the plastic potential has been selected with the same mathematical expression of the yield surface, differing from it through the variable m_ψ (i.e., when $m_\psi \equiv m_b$ the model is associated):

$$g = \frac{q^{1/a}}{\sigma_{ci}^{(1/a-1)}} + A(\theta)\frac{q}{3}m_\psi - m_\psi p\,. \qquad (3)$$

The degradation of the rock mass due to shearing has been simulated through a hyperbolic decreasing of the material properties (i.e., the hardening variables α_j of the model) by considering the following hardening rule:

$$\boldsymbol{\alpha} = \begin{Bmatrix} m_b \\ s \end{Bmatrix} = \begin{Bmatrix} m_{b_i} - \left(\frac{m_{b_i} - m_{b_r}}{B_m + \varepsilon_{eq}^p}\right)\varepsilon_{eq}^p \\ s_i - \left(\frac{s_i - s_r}{B_s + \varepsilon_{eq}^p}\right)\varepsilon_{eq}^p \end{Bmatrix}, \qquad (4)$$

$$\varepsilon_{eq}^p = \int_0^t \dot{\varepsilon}_q^p\, dt\,. \qquad (5)$$

In these equations, the subscripts i and r refer to the initial and the residual values of the corresponding variable. $\dot{\varepsilon}_q^p$ represents the increment of deviatoric plastic strain (i.e., $\dot{\varepsilon}_q^p = \sqrt{2(\dot{\varepsilon}_{s_{ij}}^p \dot{\varepsilon}_{s_{ij}}^p)/3}$, where $\varepsilon_{s_{ij}}^p = \varepsilon_{ij}^p - \frac{\varepsilon_v^p \delta_{ij}}{3}$ and ε_v^p are the deviator component of the plastic strain and the volumetric plastic strain, respectively) and the equivalent plastic strain ε_{eq}^p is its cumulated value. Consistently with Eq. 4, the same hyperbolic function has been introduced in the variable m_ψ to simulate the non-linear trend of volumetric strain in the brittle regime (El Moustapha, 2014):

$$m_\psi = m_{\psi_i} - \left(\frac{m_{\psi_i} - m_{\psi_r}}{B_\psi + \varepsilon_{eq}^p}\right)\varepsilon_{eq}^p. \qquad (6)$$

In Eqs. 4 and 6, the parameters B_m and B_s govern the rate of softening resulting from deviatoric shearing while B_ψ dictates the rate of dilation after initial yielding. The hardening rule reported in Eq. 4 is plotted in Fig. 1 to highlight how the parameters B_m, B_s and B_ψ (i.e., the parameters B_j) enforce a given rate of decay on the corresponding hardening variables.

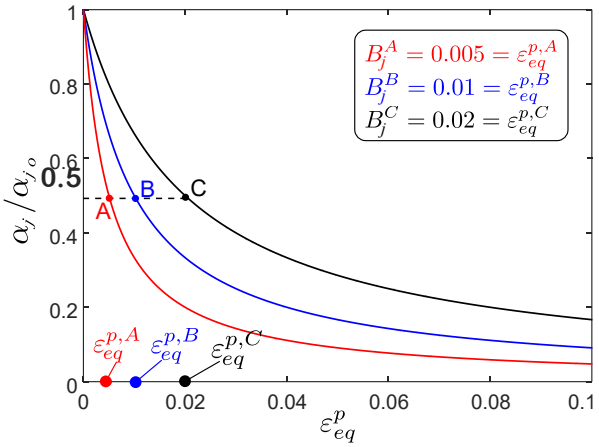

Figure 1: Evolution of the hardening variables as a function of the equivalent plastic strain. The letters A, B, C indicate the value of ε_{eq}^{p} corresponding to 50% of the corresponding initial hardening variable for three different values of B_j (i.e., B_j^A=0.005, B_j^B = 0.01 B_j^C = 0.02).

By observing Fig. 1, it is worth remarking that B_j=ε_{eq}^{p} is the specific value for which the decaying evolution of α_j reaches the 50% of its corresponding initial variable (i.e., $\alpha_j = 0.5\,\alpha_{j_o}$). For this reason, smaller values of B_j involve a faster decrease of α_j, thus resulting to a more important decrease of the material strength.

3. MODEL CALIBRATION

To test the performance of the HBS model, a first-order calibration has been proposed to simulate the post-peak regime of a porous sandstone loaded through a drained triaxial test. For this purpose, the experimental tests performed by Bésuelle et al., 2003 to investigate the mechanical behaviour of Rothbach sandstone have been considered to evaluate the initial yielding and the model characteristics during the post-peak regime. Specifically, as the experiments have been performed on the intact material, the GSI and the disturbance factor D have been selected equal to GSI = 100 and D = 0, thus having the initial values of m_b, s and a equal to m_{b_i}= m_i, s_i = 1 and $a = 0.5$, respectively. A further constitutive choice employed to reduce the number of the calibrated parameters, concerns the parameters characterizing the residual material properties which have been selected equal to zero (i.e., m_{b_r} = m_{ψ_r} = s_r = 0), thus assuming a complete material destructuration of the rock for large values of shear strain. This hypothesis simplifies the calibration process during the brittle regime, in that it assumes the post-peak response only governed by the parameters B_m, B_s and B_ψ with a resulting reduction of the number of material parameters. The performance of the resulting calibration is illustrated in Fig. 2 which shows the ability of the HBS to capture the post-peak behaviour in terms of both resistance and deformability characteristics for the set of parameters listed in Table 1.

Table 1 Model parameters for the HBS model used to calibrate Rothbach sandstone.

E [MPa]	8500
ν [-]	0.17
σ_{ci} [MPa]	38
m_i [-]	10
m_{ψ_i} [-]	8
B_m [-]	0.017
B_s [-]	0.017
B_ψ [-]	0.0035

By observing Fig. 2, it is possible to note that the selected calibration slightly anticipates the axial strain corresponding to the peak strength and postpones its value in proximity of the minimum of volumetric strain. This trend of behaviour is explained by the fact that the model neglects the presence of dissipative phenomena due to micro-cracking growth and homogeneous cements debonding occurring before the peak stress, thus considering a linear elastic response until the peak. Moreover, it is worth remarking that the proposed set of parameters results from material point analyses, thus neglecting the strong non-homogeneous strain-field consequent from the appearing of strain localization phenomena in the sample.

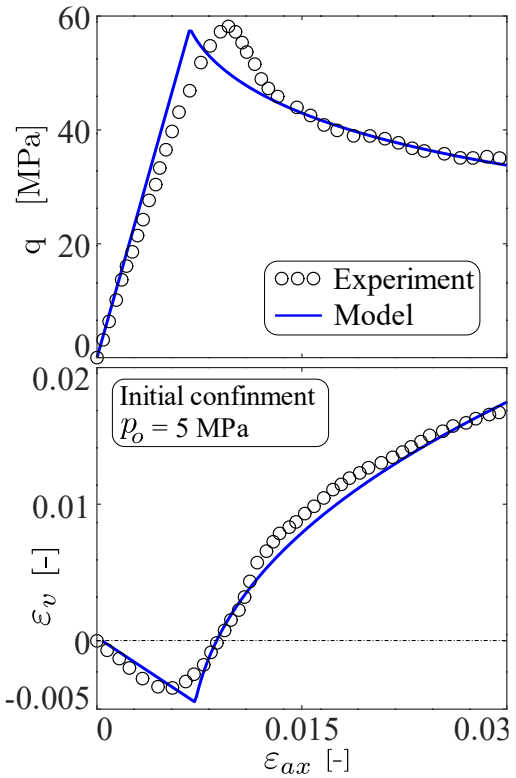

Figure 2: Calibration of the HBS model against the mechanical behaviour of Rothbach sandstone tested with a drained triaxial test performed at 5 MPa of initial confining pressure (data after Bésuelle et al., 2003).

For this reason, although the underlying calibration enables a first order estimation for the value of the model parameters, a rigorous calibration process in the brittle regime should implement an inverse analysis method which compares full-field experimental data with the numerical solution of the experimental test simulated as an initial boundary value problem (El Moustapha, 2014; Bésuelle and Lanatà, 2017).

4. PARAMETRIC ANALYSES

To investigate the effect of the model parameters during the post-peak response, sensitivity studies have been performed through a set of drained biaxial tests (BXD)

performed at 5 MPa of initial confining pressure. Specifically, the parameters tested in these analyses are *i)* the parameter m_i which prescribes the shape of the elastic domain, *ii*) the parameter m_{ψ_i} which influences the evolution of volumetric strains in the post-peak regime, *iii*) the parameters B_m and B_ψ governing the rate of softening and the rate of dilation, respectively. The numerical results are presented in Figs. 3-6, where the parameters used to simulate Rothbach sandstone are employed as a reference set of parameters and they are reported with a blue line.

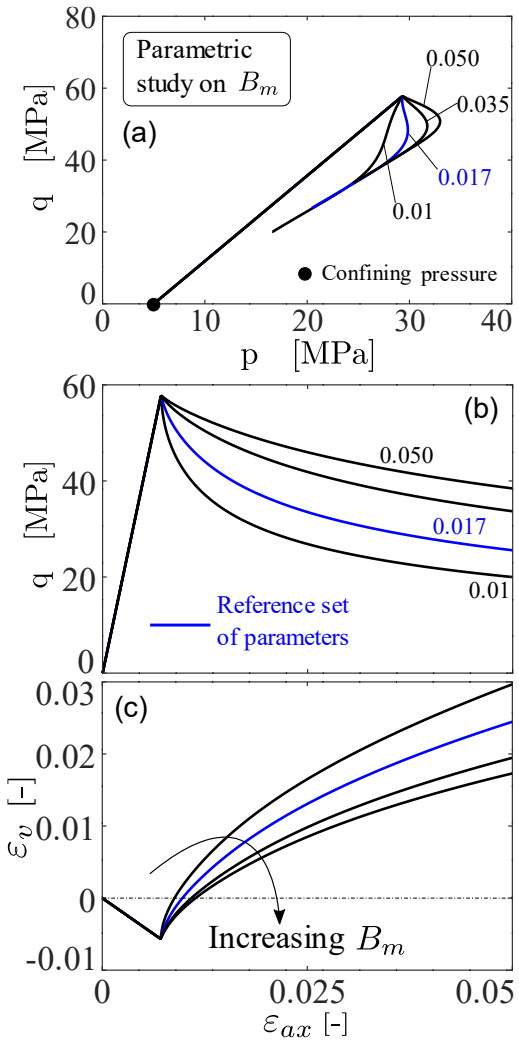

Figure 3: Sensitivity study performed on the parameter B_m through a set of drained biaxial test (BXD) performed at 5 MPa of initial confining pressures: (a) stress paths, (b) stress-strain response, (c) evolution of volumetric strain. The blue line indicates the solution of the stress path computed with the reference set of parameters reported in Table 1.

Specifically, a sensitivity study on the parameter B_m is plotted in Fig. 3 which shows the material response in terms of stress path and stress-strain response. Consistently with the plot illustrated in Fig. 1, Fig. 3 emphasizes *i)* the reduction of the strength resistance corresponding to decreasing values of B_m (Figs. 3(a)-(b)), *ii)* the influence of the softening process on the evolution of volumetric strain. As a matter of fact, it is possible to observe that the dilation trend is more accentuated for decreasing values of B_m resulting from a more important decay of the material properties (Fig. 3(c)). At variance with B_m, the parameter B_ψ has an important influence on the development of volumetric strain which for lower values of B_ψ tends to approach a regime of zero-dilation corresponding to lower values of ε_v (Fig. 4). Fig. 5 shows the effect of m_i on the mechanical behaviour of the rock which results in a homothetical expansion/shrinking of q and ε_v (Figs. 5(b)-5(c)) due to the corresponding variation of the elastic domain. Analogously, Fig. 6 reports the sensitivity study on the parameter m_{ψ_i} which affects significantly the initial evolution of volumetric strain after the peak, thus bringing the material response to higher values of ε_v at the end of the loading process.

5. LOCALIZATION ANALYSES

To investigate the intrinsic capability of the selected constitutive equations to deform in narrow shear bands, the strain localization theory (Rudnicki and Rice, 1975) has been employed in this study to characterize the inception of localized strain during a given stress path.

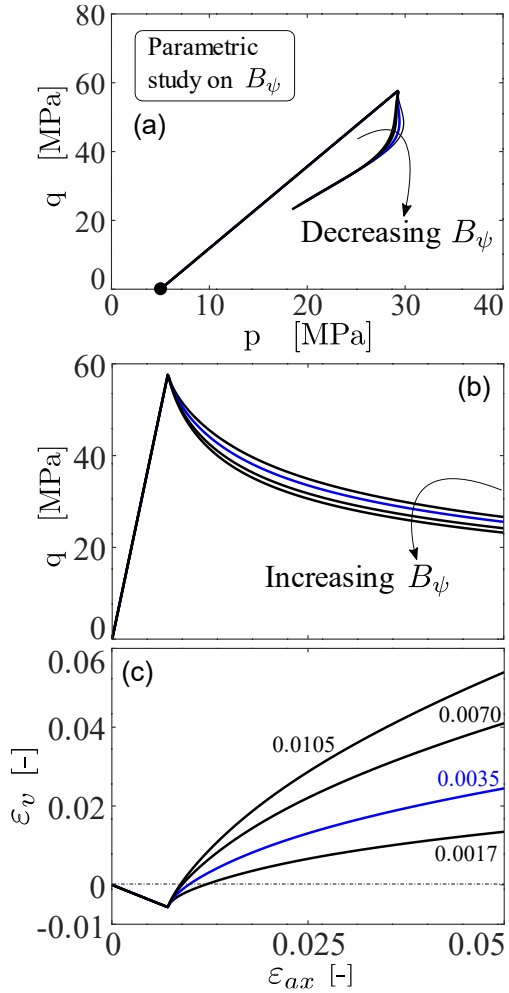

Figure 4 Sensitivity study performed on the parameter B_ψ through a set of drained biaxial test (BXD) performed at 5 MPa of initial confining pressures: (a) stress paths, (b) stress-strain response, (c) evolution of volumetric strain. The blue line indicates the solution of the stress path computed with the reference set of parameters reported in Table 1.

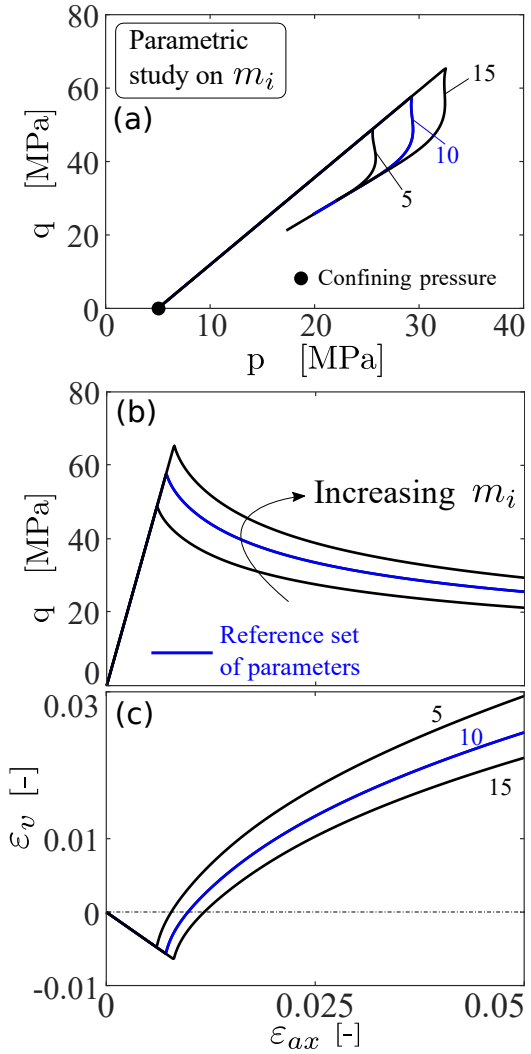

Figure 5: Sensitivity study performed on the parameter m_i through a set of drained biaxial test (BXD) performed at 5 MPa of initial confining pressures: (a) stress paths, (b) stress-strain response, (c) evolution of volumetric strain. The blue line indicates the solution of the stress path computed with the reference set of parameters reported in Table 1.

For elastoplastic constitutive equations, a criterion to identify bifurcated solutions in the form of narrow shear bands can be written as:

$$\mathcal{L}(\varphi) \leq \det\left[n_j(\varphi)\mathbb{C}^{ep}_{ijkl}n_l(\varphi)\right],$$

where $\mathbb{C}^{ep}_{ijkl}$ is the elasto-plastic constitutive tensor and φ is the angle defining the unit vector n_j orthogonal to the band (Fig. 7). In particular, although all the angles satisfying the condition reported in Eq. 7 are susceptible to predict strain localization, to evaluate the effective angle at which the strain localizes, reference will be made to the angle $\bar{\varphi}$ corresponding to the minimum of the localization criterion $\mathcal{L}(\varphi)$ (i.e., the angle φ at which $\min(\mathcal{L}) = \mathcal{L}(\bar{\varphi})$ as illustrated in Fig. 7).

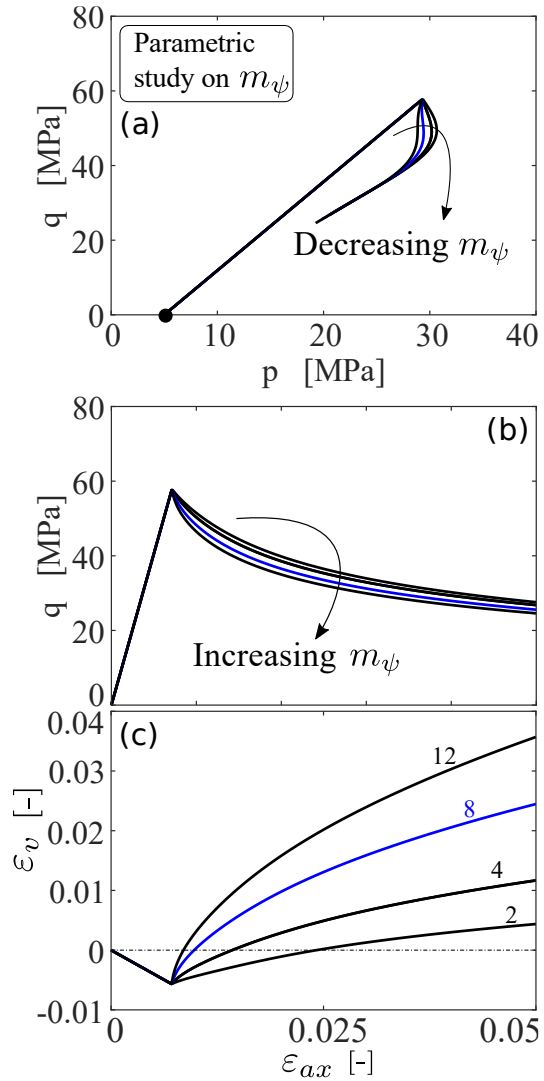

Figure 6: Sensitivity study performed on the parameter m_{ψ_i} through a set of drained biaxial test (BXD) performed at 5 MPa of initial confining pressures: (a) stress paths, (b) stress-strain response, (c) evolution of volumetric strain. The blue line indicates the solution of the stress path computed with the reference set of parameters reported in Table 1.

This theoretical framework is here employed to explore the model performance of the HBS, thus investigating the evolution of the shear-strain characteristics during plane strain stress paths. A similar strategy is proposed by Marinelli and Buscarnera (2015) and Papazoglou et al., 2017 in which the strain localization theory is used as a further tool to calibrate the mechanical response of porous rocks in the compaction regime.

The results are shown in Fig. 8 where the evolution of the localization angle $\bar{\varphi}$ is plotted as a function of the prescribed axial strains. From this figure, it is possible to observe that, for a given confining pressure p_o, there is a decreasing evolution of the angle $\bar{\varphi}$, which indicates a rotation of the shear band during the loading process.

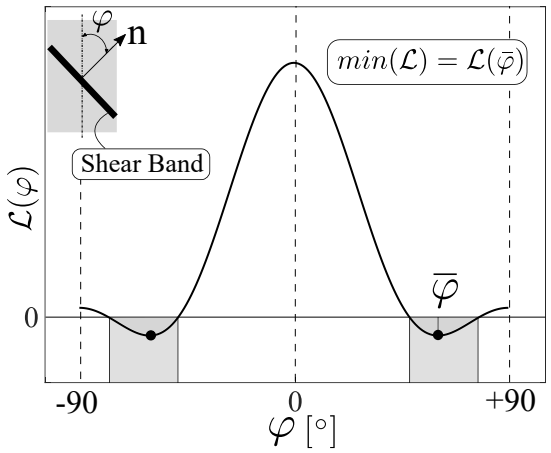

Figure 7: Plot of the bifurcation criterion $\mathcal{L}(\varphi)$ for the HBS model.

In this context, the initial confining pressure p_o has mainly two effects on the localization angle $\bar{\varphi}$: *i)* for increasing values of p_o, the range of rotations between the initial yielding and the end of the loading tends to decrease, *ii)* for increasing values of p_o, the angle $\bar{\varphi}$ at first yielding shows a decreasing trend as reported by the red line in Fig. 8. The results shown in Fig. 8 are consistent with the experimental evidence which report a decrease of the band angle inclination for higher values of the confining pressure, especially if the stress path approaches the transition from brittle-dilation to ductile compaction behaviour (Wong et al., 1997; Wong and Baud, 2012).

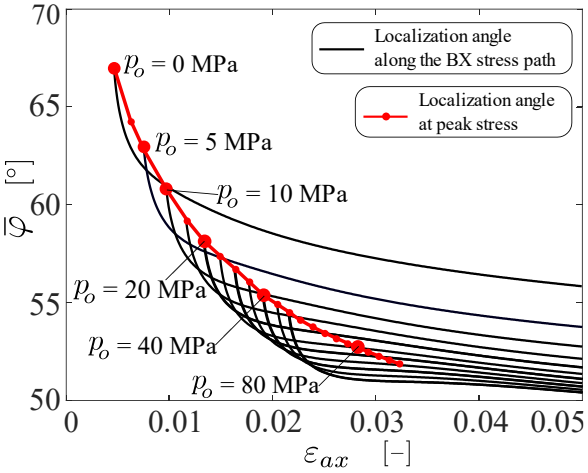

Figure 8: Evolution of the shear band angle $\bar{\varphi}$ during a biaxial stress path (BXD). The tests are controlled through the axial strain ε_{ax} and are repeated for different values of the initial confining pressure p_o by using the set of parameters reported in Table 1. The red line represents the shear band inclination at the inception of strain localization.

Moreover, the band angle inclinations are consistent with the experimental results presented in El Moustapha, 2014; Lanatà, 2015 in which biaxial stress experiments are performed on Vosges sandstone, a porous rock characterized by the same initial porosity of Rothbach sandstone (i.e., the experiments show a band inclination of 60° and 54° for a radial confinement of p_o = 20 MPa and p_o = 30 MPa, respectively).

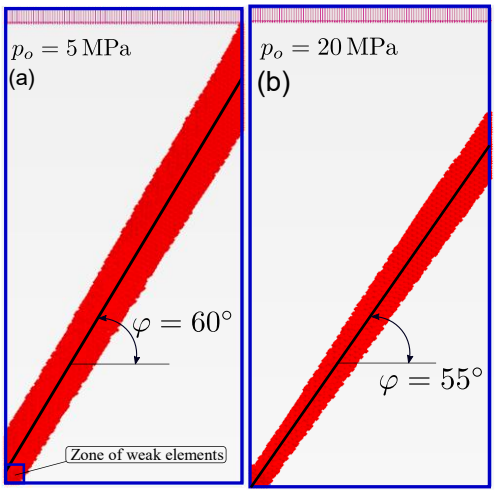

Figure 9: Gauss points distribution calculated with PLAXIS 2D to solve biaxial tests at two initial confining pressures of 5 MPa and 20 MPa

As a further validation, the shear band angles calculated with the strain localization theory have been compared with the numerical results obtained with the finite element code PLAXIS 2D with which two biaxial tests have been solved at 5 MPa and 20 MPa of initial confinement, respectively. To trigger the formation of a shear band and avoiding an initial homogeneous plastic state, a squared zone characterized by a smaller value of the uniaxial compression (i.e., $\sigma_{ci} = 37$ MPa) has been prescribed in the bottom-left corner of the sample. The results are shown in Fig. 9, where the distribution of the Gauss points in plastic loading at the inception of strain localization have been plotted with a red symbol. The inclination of the shear band has been measured with the post-processing tools available in PLAXIS 2D Output and the results show values consistent with the band angles predicted by the strain localization theory for both the initial confining pressures (Fig. 9).

To avoid the pathological mesh sensitivity characteristics of classical continuum models, a viscous regularization technique has been employed to restore the objectivity of the numerical solution during the shear band formation (Sluys, 1992). This approach has been successfully used by several authors in the compaction regime (Das and Buscarnera, 2014; Shahin et al., 2019) and will be here employed to regularize the numerical problem during brittle failure. For this purpose, the inviscid model presented in Eqs. (1)-(6), has been replaced within a rate-dependent framework based on the overstress theory proposed by Perzyna 1966, in which the visco-plastic strains are calculated through a viscous nucleus function $\Phi(f)$ according to the equation: $\varepsilon_{ij}^{vp} =< \Phi > \partial g/\partial \sigma_{ij}$. In this study, the following expression of the viscous nucleus has been used: $\Phi = \mu(< f >/\sigma_{ci})$, where μ

represents a fluidity parameter, and < >, the McCauley brackets. The global mechanical response of the sample shown in Fig. 9(b) is illustrated in Fig. 10 where the sample behavior is expressed as a function of the vertical reaction R_y and the normalized displacement $u_y \backslash u_{y,tot}$. The total value of the applied displacements $u_{y,tot}$ has been considered equal to $u_{y,tot} = 5\ cm$, while a fluidity μ has been prescribed equal to $\mu = 1.15 * 10^{-5} \backslash s$.

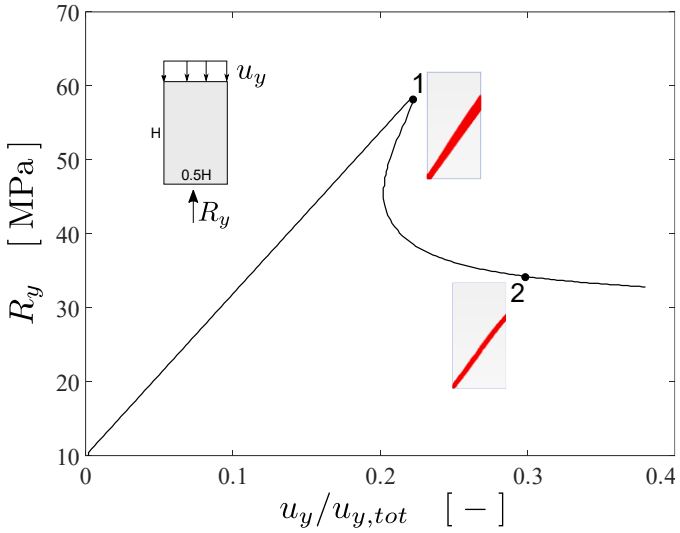

Figure 10: Global trend of behavior of the rock sample tested through a drained biaxial computation with an initial confining of 20 MPa. A value of 1 m has been considered for the height H of the sample.

6. CONCLUSIONS

This paper has discussed an elasto-plastic model based on a HB failure criterion in which a hyperbolic softening rule has been implemented to consider the material properties degradation during the post-peak regime. Specifically, the expression of the softening rule has been expressed as a function of an equivalent plastic strain (i.e., a cumulated value of the norm of deviatoric plastic strains), thus obtaining a residual strength resistance for large strains. The presented constitutive framework has been enriched by introducing a non-associated plastic potential which conserves the same mathematical expression of the yield criterion but differs from it through the variable m_ψ (i.e., when $m_\psi \equiv m_b$ the model is associated). Furthermore, to enable an accurate description of volumetric strain during the post-peak regime, the same hyperbolic function implemented for the hardening variable has been also introduced for m_ψ. The performance of the model has been investigated *i)* by calibrating the material parameters to simulate the mechanical behaviour of Rothbach sandstone, *ii)* by performing sensitivity analyses to highlight the effect of the parameters governing the rate of the softening process. To further explore the capability of the HBS model in simulating failure mechanisms with dilatant shear bands, the strain localization theory has been employed to calculate the shear band inclination of potential strain localization phenomena. The results predicted by the strain localization theory have been confirmed by numerical computations performed with the finite element code PLAXIS 2D in which biaxial tests have been solved as an IBVP. The enhanced constitutive framework based on a HB yield criterion opens the avenue to improve the analyses of geoengineering systems in which an accurate description of the failure mechanisms represents a crucial ingredient to guarantee more reliable design strategies.

REFERENCES

1. Alejano, L., E. Alonso, A. Rodríguez-Dono and G. Fernández-Manín. 2010. Application of the convergence-confinement method to tunnels in rock masses exhibiting hoek-brown strain softening behaviour. International Journal of Rock Mechanics and Mining Sciences, 47(1):150-160.
2. Barnichon, J.-D. 1998. Finite Element Modelling in Structural and Petroleum Geology. PhD thesis, Université de Liège Faculté des Sciences Appliquées.
3. Collin, F. 2003. Couplages thermo-hydro-hydro-méchanique dans les sols et les roches tendres partiellement saturé (Ph.D. thesis), Université de Liège, Faculté de Science Appliquèes.
4. Bésuelle, P., P. Baud and Wong, T.-F. 2003. Failure mode and spatial distribution of damage in Rothbach sandstone in the brittle-ductile transition. In Kümpel, H.-J., editor, Thermo-Hydro-Mechanical Coupling in Fractured Rock, Pageoph Topical Volumes, pages 851-868. Birkhäuser Basel.
5. Bésuelle, P. and P. Lanatà. 2017. Emergence of strain localization in porous rocks characterized by full- eld measurement in plane strain condition. In Papamichos, E., Papanastasiou, P., Pasternak, E., and Dyskin, A., editors, Bifurcation and Degradation of Geomaterials with Engineering Applications, pages 25-31, Cham. Springer International Publishing.
6. Brown, T. 2008. Estimating the mechanical properties of rock masses. In Potvin, Y., Carter, J., Dyskin, A., and Jeffrey, R., editors, Proceedings of the First Southern Hemisphere International Rock Mechanics Symposium, pages 3-22. Australian Centre for Geomechanics.
7. Cai, M. 2010. Practical estimates of tensile strength and hoek brown strength parameter mi of brittle rocks. Rock Mechanics and Rock Engineering, 43(2):167-184.
8. Cai, M. 2011. Rock mass characterization and rock property variability considerations for tunnel and cavern design. Rock Mechanics and Rock Engineering, 44(4):379-399.
9. Cai, M., P. Kaiser, H. Uno, Y. Tasaka and M. Minami. 2004. Estimation of rock mass deformation modulus and strength of jointed hard rock masses using the gsi

system. International Journal of Rock Mechanics and Mining Sciences, 41(1):3-19.

10. Carranza-Torres, C. and C. Fairhurst. 1999. The elasto-plastic response of underground excavations in rock masses that satisfy the hoek brown failure criterion. International Journal of Rock Mechanics and Mining Sciences, 36(6):777-809.

11. Das, A., Buscarnera, G., 2014. Simulation of localized compaction in high-porosity calcarenite subjected to boundary constraints. Int J Rock Mech Min Sci, 71: 91-104

12. Eberhardt, E. 2012. The hoek-brown failure criterion. Rock Mechanics and Rock Engineering, 45(6):981 988.

13. El Moustapha, K. 2014. Identification de lois de comportement enrichies pour les géomatériaux en présence d'une localisation de la déformation. PhD thesis, Université de Grenoble, Laboratoire 3SR, Equipe GDR.

14. El Moustapha, K., P. Besuelle, Y. Sieffert, and R. Chambon. 2013. Identification d'une loi de comportement enrichie pour les géomatériaux en présence d'une localisation de la déformation. In 21ème Congrès Français de mécanique [CFM2013]. AFM, Maison de la Mécanique, 39/41 rue Louis Blanc, 92400 Courbevoie, France.

15. Hoek, E. 1983. Strength of jointed rock masses. Géotechnique, 33(3):187-223.

16. Hoek, E. 1990. Estimating mohr-coulomb friction and cohesion values from the hoek-brown failure criterion. International Journal of Rock Mechanics and Mining Sciences & Geomechanics Abstracts, 27(3):227-229.

17. Hoek, E. and E. Brown. 1997. Practical estimates of rock mass strength. International Journal of Rock Mechanics and Mining Sciences, 34(8):1165-1186.

18. Hoek, E., C. Carranza-Torres and B. Corkum. 2002. Hoek-brown failure criterion. In Proceedings of the 5th North American Rock Mechanics Symposium, pages 267-273.

19. Jiang, H. and J. Zhao. 2015. A simple three-dimensional failure criterion for rocks based on the hoek-brown criterion. Rock Mechanics and Rock Engineering, 48(5):1807-1819.

20. Lanatà, P., 2015. Full-field experimental characterization of mechanical behaviour and failure in porous rock in plane strain compression: homogeneous deformations and strain localization. Ph.D. Thesis, Laboratoire 3SR, Grenoble, FR.

21. Lin, Q., P. Cao and P. Wang. 2018. Study of post-peak strain softening mechanical behaviour of rock material based on hoek-brown criterion. Advances in Civil Engineering.

22. Marinelli, F. and G. Buscarnera. 2015. Parameter calibration for high-porosity sandstones deformed in the compaction banding regime. International Journal of Rock Mechanics and Mining Sciences, 78(0):240-252.

23. Marinos, V., P. Marinos and E. Hoek. 2005. The geological strength index: applications and limitations. Bulletin of Engineering Geology and the Environment, 64(1):55-65.

24. Martin, C. D., P. K. Kaiser and D. R. McCreath. 1999. Hoek-brown parameters for predicting the depth of brittle failure around tunnels. Canadian Geotechnical Journal, 36(1):136-151.

25. Papazoglou A., Shahin G., Marinelli F., Dano C., Buscarnera G., Viggiani G. (2017) Localized Compaction in Tuffeau de Maastricht: Experiments and Modeling. In: Papamichos E., Papanastasiou P., Pasternak E., Dyskin A. (eds) Bifurcation and Degradation of Geomaterials with Engineering Applications. IWBDG 2017. Springer Series in Geomechanics and Geoengineering. Springer, Cham

26. Perzyna, P., 1966. Fundamentals problems in visco-plasticity. Advances in applied mechanics, 9: 243-377.

27. Rudnicki, J. and J. Rice. 1975. Conditions for the localization of deformation in pressure sensitive dilatant materials. Journal of the Mechanics and Physics of Solids, 23(6):371-394.

28. Shahin, G., Papazoglou, A., Marinelli, F., Buscarnera, G. 2019. Simulation of localized compaction in Tuffeau de Maastricht based on evidence from X-ray tomography (under review).

29. Sluys, L. J., 1992. Wave propagation, localization and dispersion in softening solids. Ph.D. Thesis, Delft University of Technology.

30. Wong, T.-F. and P. Baud. 2012. The brittle-ductile transition in porous rock: A review. Journal of Structural Geology, 44(0):25-53.

31. Wong, T.-f., C. David and W. Zhu. 1997. The transition from brittle faulting to cataclastic flow in porous sandstones: Mechanical deformation. Journal of Geophysical Research: Solid Earth, 102(B2):3009-3025.

32. Zhao, X. and M. Cai. 2010. Influence of plastic shear strain and confinement-dependent rock dilation on rock failure and displacement near an excavation boundary. International Journal of Rock Mechanics and Mining Sciences, 47(5):723-738.

33. Zou, J.-f., S.-q. Zuo and Y. Xu. 2016. Solution of strain-softening surrounding rock in deep tunnel incorporating 3d hoek-brown failure criterion and flow rule. Mathematical Problems in Engineering.